Stem Cell Reports
Article
ISSCR
OPEN ACCESS

# Mitoregulin Controls β-Oxidation in Human and Mouse Adipocytes

Max Friesen,[1,7] Curtis R. Warren,[2,7] Haojie Yu,[1,7] Takafumi Toyohara,[1,7] Qiurong Ding,[3] Mary H.C. Florido,[1] Carolyn Sayre,[1] Benjamin D. Pope,[1,4] Loyal A. Goff,[5] John L. Rinn,[6] and Chad A. Cowan[1,*]

[1]Division of Cardiovascular Medicine, Department of Medicine, Beth Israel Deaconess Medical Center, Boston, MA 02115, USA
[2]Cardiometabolic Disease Research, Boehringer-Ingelheim Pharmaceuticals Inc., Ridgefield, CT 06877, USA
[3]CAS Key Laboratory of Nutrition and Metabolism, Institute for Nutritional Sciences, Shanghai Institutes for Biological Sciences, Chinese Academy of Sciences, University of Chinese Academy of Sciences, Shanghai 200031, P.R. China
[4]Disease Biophysics Group, Wyss Institute for Biologically Inspired Engineering, John A. Paulson School of Engineering and Applied Sciences, Harvard University, Cambridge, MA 02138, USA
[5]McKusick-Nathans Institute of Genomic Medicine, Johns Hopkins University, Baltimore, MD 21205, USA
[6]University of Colorado Boulder, Boulder, CO 80303, USA
[7]Co-first author
*Correspondence: chad_cowan@harvard.edu
https://doi.org/10.1016/j.stemcr.2020.03.002

## SUMMARY

We previously discovered in mouse adipocytes an lncRNA (the homolog of human *LINC00116*) regulating adipogenesis that contains a highly conserved coding region. Here, we show human protein expression of a peptide within *LINC00116*, and demonstrate that this peptide modulates triglyceride clearance in human adipocytes by regulating lipolysis and mitochondrial β-oxidation. This gene has previously been identified as mitoregulin (*MTLN*). We conclude that *MTLN* has a regulatory role in adipocyte metabolism as demonstrated by systemic lipid phenotypes in knockout mice. We also assert its adipocyte-autonomous phenotypes in both isolated murine adipocytes as well as human stem cell-derived adipocytes. *MTLN* directly interacts with the β subunit of the mitochondrial trifunctional protein, an enzyme critical in the β-oxidation of long-chain fatty acids. Our human and murine models contend that *MTLN* could be an avenue for further therapeutic research, albeit not without caveats, for example, by promoting white adipocyte triglyceride clearance in obese subjects.

## INTRODUCTION

Computational annotation of coding genes in the human genome is complicated by myriad non-functional small open reading frames (smORFs) created by random in-frame linking of start and stop codons (Collins and Mansoura, 2001; Venter et al., 2001). For this reason, algorithms predicting coding genes use a minimum of 100 codons, because existing tools cannot discern translated from non-protein-encoding smORFs, resulting in the misclassification of some small coding genes as long non-coding RNAs (lncRNAs). More recently, codon substitution frequency has been used to predict protein-encoding transcripts within lncRNA catalogs (Cabili et al., 2011; Guttman and Rinn, 2012). These analyses suggest the putative existence of thousands of smORF-encoded peptides (SEPs) in the human proteome, many with functional significance in human biology (Anderson et al., 2015; D'Lima et al., 2017; Lee et al., 2015; Matsumoto et al., 2017). Proteomics data suggest that hundreds of these SEPs may be expressed by human cells (Slavoff et al., 2013). Here, we characterized *MTLN*, an adipocyte-expressed SEP encoded by *LINC00116*. *MTLN* has twice previously been described as a mitochondrial regulator of fatty acid oxidation through the mitochondrial trifunctional protein (Makarewich et al., 2018; Stein et al., 2018). Both groups focused on murine muscle, showing changes in mitochondrial respiration upon *MTLN* knockout (KO). *MTLN* also regulates C2C12 myoblast differentiation through enhancing mitochondrial respiration (Lin et al., 2019). One of the proteins *MTLN* interacts with is Cyb5r3, which is one potential way it is regulating lipid metabolism (Chugunova et al., 2019).

However, *MTLN* is also present in adipose tissue, an important locus of energy homeostasis with high rates of fatty acid metabolism. Adipose tissue comprises an endocrine organ responsible for the storage of excess nutrients in the form of triglycerides (TGs) and mobilization of these energy stores as free fatty acids (FFAs) (Pope et al., 2016). Adipocytes liberate FFAs and glycerol from intracellular TG stores in response to starvation by a mechanism known as lipolysis and secrete these products into the bloodstream for use as fuel by other tissues. Mitochondria catabolize FFAs to produce ATP in a process known as β-oxidation (Roberts et al., 2014). It is postulated that induction of uncoupled mitochondrial respiration in adipocytes (a process referred to as adipocyte browning) could serve as a therapeutic approach to obesity (Moisan et al., 2015). An orthogonal approach would be to augment clearance of fatty acids by mitochondrial β-oxidation. We have explored *MTLN*'s function in lipolysis and β-oxidation using human pluripotent stem cell (hPSC)-derived adipocytes (Lee and Cowan, 2014) as well as murine models.

This approach is very powerful due to the ease with which one can differentiate hPSCs into any desired tissue, and the possibility of genetic manipulation. In addition, any study into human disease or biology is well served


This is an open access article under the CC BY-NC-ND license (http://creativecommons.org/licenses/by-nc-nd/4.0/).

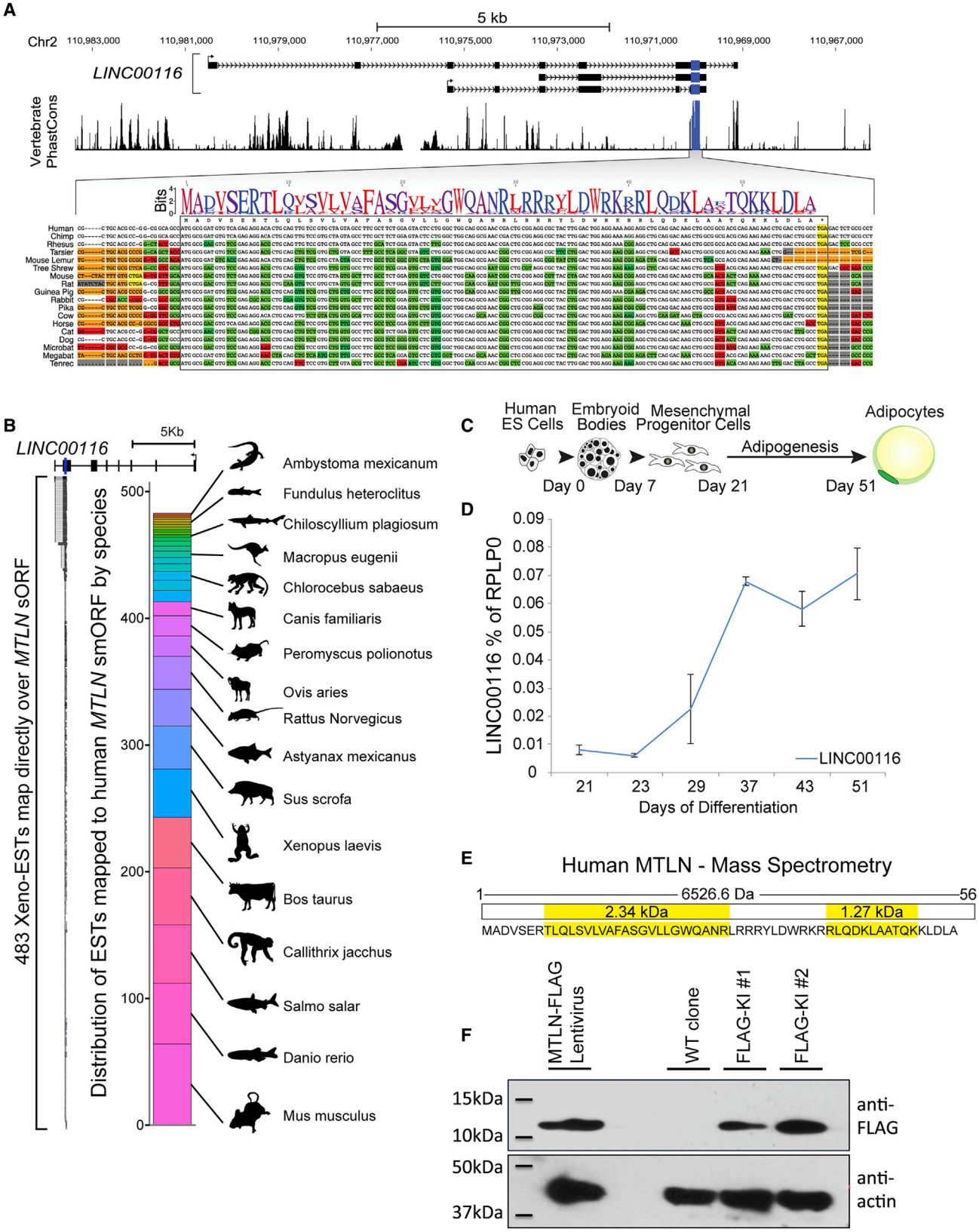


*(legend on next page)*

by using a human model system. We have exploited these features to study *MTLN* in human adipocytes with normal, heightened, or abrogated *MTLN* expression. This approach revealed the mechanism by which *MTLN* regulates β-oxidation through its physical presence in mitochondria.

## RESULTS

### Identification of *MTLN* in Human Adipocytes

The mouse non-coding RNA *1500011K16Rik*, Lnc-RAP5 in the original study, exerts control over lipid accumulation in differentiating mouse pre-adipocytes (Sun et al., 2013). This lncRNA harbors the putative 56-codon *MTLN* smORF, raising the possibility that the effect on adipocyte function could be driven by either the lncRNA or the encoded SEP. This smORF is conserved in the human homolog of *1500011K15Rik*, known as *LINC00116* (Figure 1A). Nucleotide and amino acid pairwise identity of this smORF among placental mammals (89.8% and 94.8%, respectively) together with a strong PhyloCSF score (562.72) suggested that the smORF encodes a protein (Lin et al., 2011). This high degree of codon-level conservation is not observed in the immediate flanking regions or elsewhere within the host lncRNA. Evolutionary conservation of the smORF is demonstrated further by 483 annotated expressed sequence tags from 33 vertebrate species that map directly over the human smORF (Figure 1B).

To evaluate expression of this smORF in a human adipocyte model, we differentiated hPSC-derived mesenchymal progenitor cells (MPCs) to white adipocytes (hPSC-adipocytes) (Figure 1C). *LINC00116* mRNA expression continually increases over 30 days of adipogenesis (Figure 1D). After confirming expression of the *LINC00116* mRNA in hPSC-adipocytes, we sought to verify translation of the *MTLN* peptide. Mass spectrometry of whole-cell lysate from hPSC-adipocytes identified two tryptic peptides (2.34 and 1.27 kDa) derived from *MTLN* (Figures 1E, S1C, and S1D). In an orthogonal approach, we used CRISPR/Cas9-mediated genome editing to knock in a FLAG tag at the C terminus of the endogenous *MTLN* gene in the human embryonic stem cell line HUES9 (Figures S1A and S1B). Immunoblotting for the endogenous *MTLN*-FLAG or an exogenous lentivirus-delivered *MTLN*-FLAG identified a peptide of >10 kDa, which is not present in parental wild-type (WT) control cells (Figures 1F, S1E, and S1F). Together, these data verify that *MTLN* is a bona fide SEP encoded by the conserved smORF in *LINC00116*.

### MLTN Knockout Regulates Blood Lipid Levels in Mice

To directly address the physiological role of *MTLN* in metabolic regulation, we generated *MTLN* loss-of-function mice by targeting the mouse homolog of *MTLN* harbored by *1500011K16Rik* using CRISPR/Cas9-mediated genome editing (Figure S2A). The resultant $MTLN^{-/-}$ mouse strain carries a 5-base pair deletion at the N terminus of the *MTLN* smORF (Figure S2B). This mutation does not affect expression of the lncRNA transcript *1500011K16Rik* in liver, brown adipose tissue, or gonadal white adipose tissue (Figure 2A).

High-fat diets (HFDs) are used to assess metabolic dysfunction in mice, and adipose phenotypes are often uncovered and exacerbated by this feeding regimen. $MTLN^{-/-}$ mice were challenged with HFD to assess the effects of *MTLN* depletion on lipid handling. During HFD, circulating TG levels were decreased in both male and female $MTLN^{-/-}$ mice compared with WT littermates (Figure 2B). Serum total cholesterol and FFAs also were decreased in female and male $MTLN^{-/-}$ mice, respectively (Figures 2C and 2D). Despite these differences in blood lipid concentrations, there was no change in body weight between $MTLN^{-/-}$ and WT littermates (Figure S2C). On normal chow diet, global depletion of *MTLN* reduced serum total cholesterol level in female mice (Figure S2E), but had no effect on circulating TG (Figure S2D) or FFA (Figure S2F).

### *MTLN* Regulates TG Accumulation and Metabolism in Murine and Human Adipocytes

HFD experiments using $MTLN^{-/-}$ mice demonstrated that circulating lipid levels are affected by global *MTLN*

**Figure 1. Identification of a Conserved SEP Expressed by Adipocytes**

(A) Alignment of *LINC00116*'s conserved smORF and its homologs from 18 placental mammals, including translation of the SEP.

(B) A total of 483 expressed sequence tags (ESTs) from 33 distinct vertebrate species map over the human *MTLN* smORF. The distribution of the number of ESTs by species is shown. Xeno-ESTs are derived from translated BLAT alignments of ESTs in GenBank from non-human vertebrates (UCSC "xenoEst" track).

(C) Protocol for differentiation of hPSC-adipocytes. Adipogenesis begins with MPCs on day 21 of the protocol.

(D) qRT-PCR analysis of *LINC00116* mRNA levels throughout adipogenesis. n = 3 independent biological replicate experiments.

(E) Primary sequence of the *MTLN* peptide. Peptides identified by mass spectrometry analysis of hPSC-adipocytes with their respective molecular weights in yellow.

(F) Immunoblot of whole-cell lysate from *MTLN*-FLAG knockin hPSC-adipocytes and lentivirus-delivered *MTLN*-FLAG-overexpressing hPSC-adipocytes. β-Actin was used as the loading control.

Data are means ± SD. Related to Figure S1.

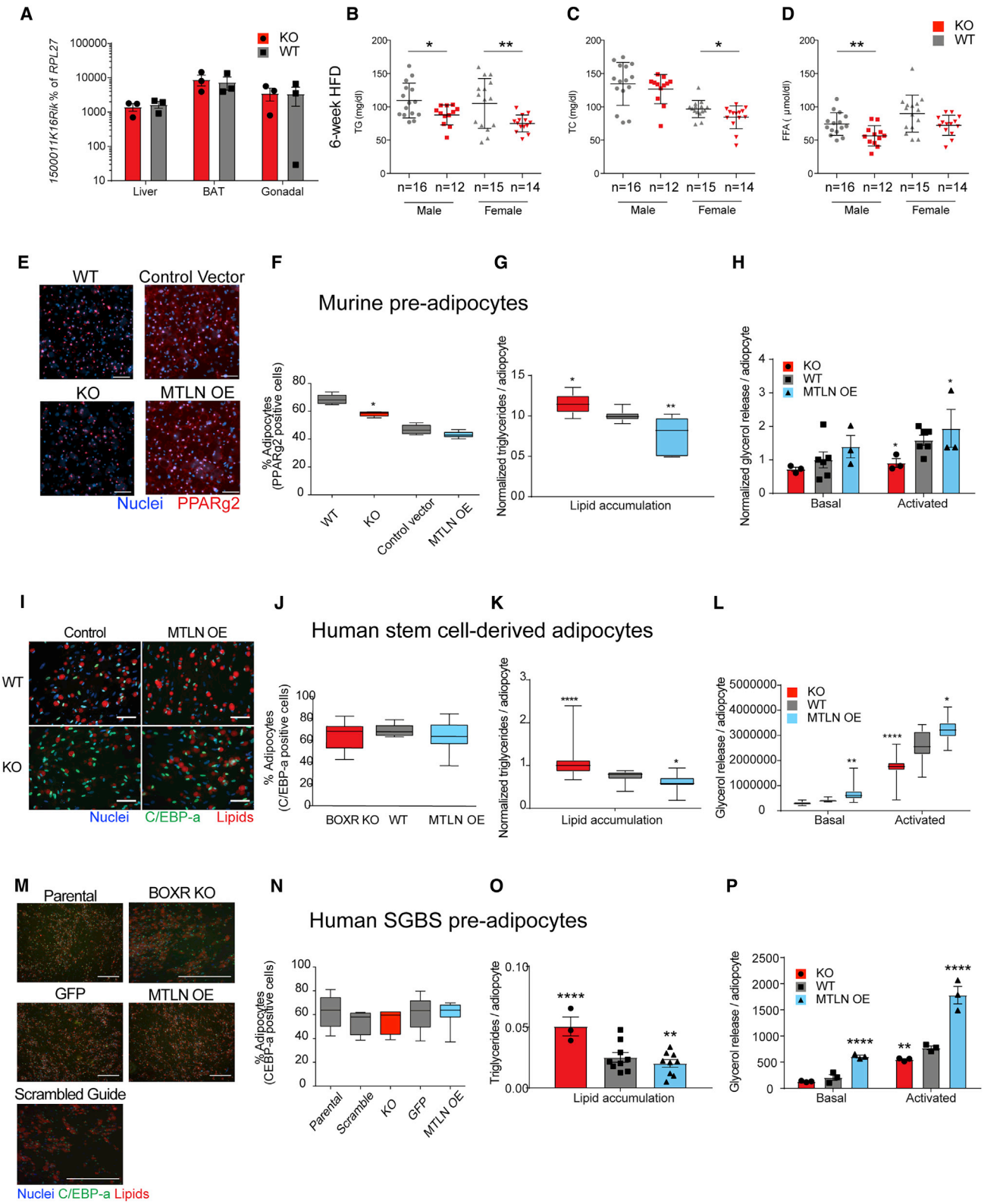


*(legend on next page)*

depletion. To investigate the adipocyte-autonomous effects of *MTLN*, we isolated murine pre-adipocytes from WT and *MTLN*$^{-/-}$ mice. Loss of *MTLN* led to a mild decrease in differentiation efficiency as measured by PPARg2, although overexpression of *MTLN* had no effect (Figures 2E and 2F). *MTLN* did have a significant effect on TG accumulation, leading to increased lipid in the KO, and reduced TGs in the *MTLN*-overexpressing (OE) cells (Figure 2G). Consistent with this phenotype *MTLN* also affected forskolin-activated lipolysis in murine adipocytes, which was lower in the KO and higher in the OE cells (Figures 2H and S2K). These results suggest that *MTLN* has an adipocyte-autonomous effect on lipid handling.

To investigate the human-specific effects of *MTLN*, we created *MTLN* KO hPSCs by leveraging CRISPR/Cas9 genome editing (Figure S2G). The resulting four KO hPSC clones contain homozygous frameshift mutations in the *MTLN* smORF (Figure S2H). Overexpression of *MTLN* (Figure S1F) persisted after lentiviral transduction of MPCs and differentiation to adipocytes. *MTLN* KO did not affect transcription of the endogenous *LINC00116* transcript (Figure S2I). We used *MTLN* KO and *MTLN* OE cells to study the effect of *MTLN* on lipid metabolism in differentiated human adipocytes.

We assessed human adipocyte differentiation efficiency by measuring the percentage of nuclei positive for the mature adipocyte marker CCAAT/enhancer binding protein alpha (Figure 2I). There was no significant difference in human adipocyte differentiation efficiency between WT, KO, or *MTLN* OE cells (Figure 2J). In contrast, *MTLN* had a significant effect on TG accumulation (Figure 2K) and lipolysis (Figures 2L and S2L). *MTLN* KO caused increased accumulation of TG, whereas *MTLN* OE resulted in a decrease in intracellular TG. In accord with this phenotype, basal lipolysis was lower in *MTLN* KO hPSC-adipocytes and increased in *MTLN* OE hPSC-adipocytes. During stimulation of lipolysis with forskolin, *MTLN* KO hPSC-adipocytes liberate fewer FFAs into the medium than WT or *MTLN* OE hPSC-adipocytes. The lipid accumulation and lipolysis phenotypes are strikingly similar between murine and human adipocytes.

Cumulatively, these results suggest that *MTLN* does not affect human adipogenesis but affects a lipolytic phenotype in human white adipocytes. To validate these findings, we replicated this set of experiments in an immortalized human pre-adipocyte cell line that readily differentiates into mature adipocytes: Simpson-Golabi-Behmel syndrome (SGBS) cells. We targeted the *MTLN* ORF using CRISPR/Cas9 to make *MTLN* KO SGBS cells (Figure S2J). In agreement with the hPSC-adipocyte phenotypes, *MTLN* KO or *MTLN* OE had no effect on SGBS differentiation efficiency (Figures 2M and 2N). TG accumulation in SGBS adipocytes was reduced by *MTLN* OE and increased by *MTLN* KO (Figure 2O). Lipolytic phenotypes of *MTLN*

**Figure 2. *MTLN* Regulates Blood Lipid Levels and Adipocyte Lipid Metabolism**

(A) qRT-PCR analysis of *1500011K16Rik* in primary mouse liver, brown adipose tissue (BAT), and gonadal adipose tissue (gWAT). n = 3 litter-matched mice, 3 technical replicates each.

(B–D) Serum triglycerides (B), total cholesterol (C), and free fatty acids (D) in mice fed a high-fat diet for 6 weeks, one matched cohort.

(E) Immunofluorescence imaging of murine pre-adipocytes stained for PPAR$\gamma$2 (red) and nuclei (blue). Scale bars, 100 μm.

(F) High-content imaging quantification of the percentage of PPAR$\gamma$2-positive nuclei in differentiated murine pre-adipocytes. n = 6.

(G) Quantification of triglyceride accumulation in differentiated murine pre-adipocytes. n = 16 for WT, 8 for KO, 7 for OE biological replicates from one differentiation.

(H) Concentration of glycerol released into the medium of differentiated murine pre-adipocytes under basal or forskolin-stimulated conditions. n = 6 for WT, 3 for KO, 3 for OE.

(I) Immunofluorescence imaging of genome-edited hPSC-adipocytes stained for C/EBP-$\alpha$ (CCAAT/enhancer binding protein alpha) (green), neutral lipids (red), and nuclei (blue). Scale bars, 100 μm.

(J) High-content imaging quantification of the percentage of C/EBP-$\alpha$-positive nuclei in differentiated hPSC-adipocytes. n = 20 for WT, 40 for KO and OE.

(K) Quantification of triglyceride accumulation in hPSC-adipocytes. n = 33 for WT, 54 for KO, 75 for OE.

(L) Concentration of glycerol released into the medium of hPSC-adipocytes under basal or forskolin-stimulated conditions. n = 30/21 for WT, 42/42 for KO, 66/90 for OE basal/stimulated.

(M) Immunofluorescence imaging of genome-edited SGBS adipocytes stained for C/EBP-$\alpha$ (green), neutral lipids (red), and nuclei (blue). Scale bars, 500 μm.

(N) High-content imaging quantification of the percentage of C/EBP-$\alpha$-positive nuclei in differentiated SGBS adipocytes. n = 9 for parental, GFP, and *MTLN* OE, 12 for *MTLN* KO and scrambled guide RNA control.

(O) Quantification of triglyceride accumulation in SGBS adipocytes. n = 9 for WT, 3 for KO, 12 for OE.

(P) Concentration of glycerol released into the medium of SGBS adipocytes under basal or forskolin-stimulated conditions. n = 3 for WT, KO, and OE.

Data are means ± SD. *p $\leq$ 0.05, **p $\leq$ 0.01, ***p $\leq$ 0.001, ****p $\leq$ 0.0001; one- or two-way ANOVA. Unless specified, "WT" groups include both untransduced and control vector overexpression cells. All n values are independent biological replicates, with 25 fields per replicate averaged for the imaging, and all lipid accumulation and glycerol release done in technical duplicate. Related to Figure S2.

KO and *MTLN* OE SGBS adipocytes were also consistent with hPSC-adipocytes (Figure 2P). The consistent phenotypes of *MTLN* KO and OE adipocytes in both murine and human models implied that the *MTLN* peptide might localize to the lipid droplet or mitochondria, the sites of lipolysis and fatty acid oxidation.

### *MTLN* Localizes to the Mitochondria and Regulates Mitochondrial Respiration

We determined the localization of *MTLN* using *MTLN*-HA and *MTLN*-FLAG OE hPSC-adipocytes by immunofluorescent confocal microscopy as well as transmission electron microscopy with immunogold labeling. Immunofluorescent labeling indicated that *MTLN* co-localizes with the mitochondrial marker hexokinase-1 (HK1) and the mitochondrial ATP synthase subunit beta (ATP5B) (Figures 3A and S3A–S3C). The immunogold-labeled *MTLN* was found at the mitochondrial membrane (Figures 3B and S3D–S3F). To verify these measures of subcellular localization, we performed cell fractionation to purify mitochondria from the nuclear and cytoplasmic fractions. HK1, ATP5B, and *MTLN*-FLAG all localized together in the mitochondrial fraction, whereas only histone H3 was present in the nuclear fraction (Figure 3C). We have been unable to generate an antibody to *MTLN*, and therefore, have only visualized the overexpressed *MTLN* constructs. Although neither the FLAG- nor HA-tag have been reported to localize to the mitochondria, we cannot fully exclude an effect of the tag on *MTLN* localization. However, our findings are consistent with previous publications localizing *MTLN* to the inner mitochondrial membrane (Makarewich et al., 2018; Stein et al., 2018).

The mitochondrial localization of *MTLN* and its effect on lipolysis and TG accumulation suggest that the peptide might affect cellular energetic pathways. To test this hypothesis, we assayed glycolysis, glucose-driven mitochondrial respiration, and fatty acid oxidation (FAO) in hPSC-adipocytes. Consistent with our previous lipolysis assays, both basal and maximal FAO were decreased in the KO and increased in the *MTLN* OE cells (Figures 3D and S3I). To compensate for this energetic imbalance, the KO displayed increased glycolysis, while the OE cells showed reduced glycolysis (Figures 3E and S3G). The KO also showed higher glycolytic capacity, while the OE showed increased glycolytic reserve. Non-FAO mitochondrial oxidative respiration was decreased in *MTLN* OE hPSC-adipocytes and increased in the KO (Figures S3H and S3J). Despite these dramatic changes in mitochondrial metabolism, we saw no evidence of adipocyte browning or increased mitochondrial content (Figures S3K and S3L). These results dovetail well with previous reports, but add a layer of complexity due to the specific regulation of fatty acid metabolism in adipocytes (Makarewich et al., 2018; Stein et al., 2018). The suppressive effect of *MTLN* on glycolysis and oxidative respiration and the increase in FAO suggests that *MTLN* causes adipocytes to favor fatty acid β-oxidation for energy production. The protein constituents of the mitochondrial β-oxidation pathway are well known, so we hypothesized that *MTLN* interacts with known β-oxidation pathway proteins.

### Interaction of *MTLN* with Key Regulators of Mitochondrial Metabolism

We affinity-purified *MTLN*-FLAG and interacting proteins from MPCs and hPSC-adipocytes to identify protein binding partners interacting with the peptide. Mass spectrometry analysis suggested that *MTLN* itself was the most highly enriched protein in both cell types, confirming the specificity of our purification strategy (Figure 4A). Gene ontology analysis of the eluted proteins' subcellular compartmentalization identified the mitochondrion as the most highly enriched cellular compartment associated with *MTLN*, secondary to translation machinery inherent to our overexpression strategy (Figure 4B). Biological processes significantly associated with *MTLN*-interacting proteins included fatty acid metabolism and oxidative phosphorylation, among other lipid and metabolite handling processes (Figure S4A). We verified the co-immunoprecipitation of exogenously expressed mitochondrial trifunctional enzyme, subunit beta (HADHB) and the endogenous ATP synthase beta subunit (ATP5B) using immunoblotting (Figures 4B, 4C, and S4B–S4D). The mitochondrial trifunctional enzyme interaction had been described earlier, but the found interaction with ATP5B seems to be a novel or adipocyte-specific process (Makarewich et al., 2018; Stein et al., 2018). As with our visualization experiments, our approach does have the drawback of only using *MTLN*-FLAG overexpression, not the endogenous gene. We compared these with samples not expressing *MTLN*-FLAG. Therefore, we followed up by restricting our analysis to adipocytes, where endogenous *MTLN* is more highly expressed, we see an even stronger bias toward mitochondrial localization and processes. This approach also removed the background inherent to our overexpression strategy. On the other hand, *MTLN*-protein interactions specific to adipocytes in our dataset almost solely localize to mitochondrial compartments (Figure 4E). Similarly, all the proteins found this way are directly involved in mitochondrial or metabolic processes (Figure 4F). The involvement of *MTLN* in mitochondrial compartments and metabolic processes, and the direct interaction between *MTLN* and ATP5B, as well as other lipid-handling proteins, such as the β subunit of the mitochondrial trifunctional enzyme, strengthen our conclusion that *MTLN* regulates lipid handling in adipocytes.

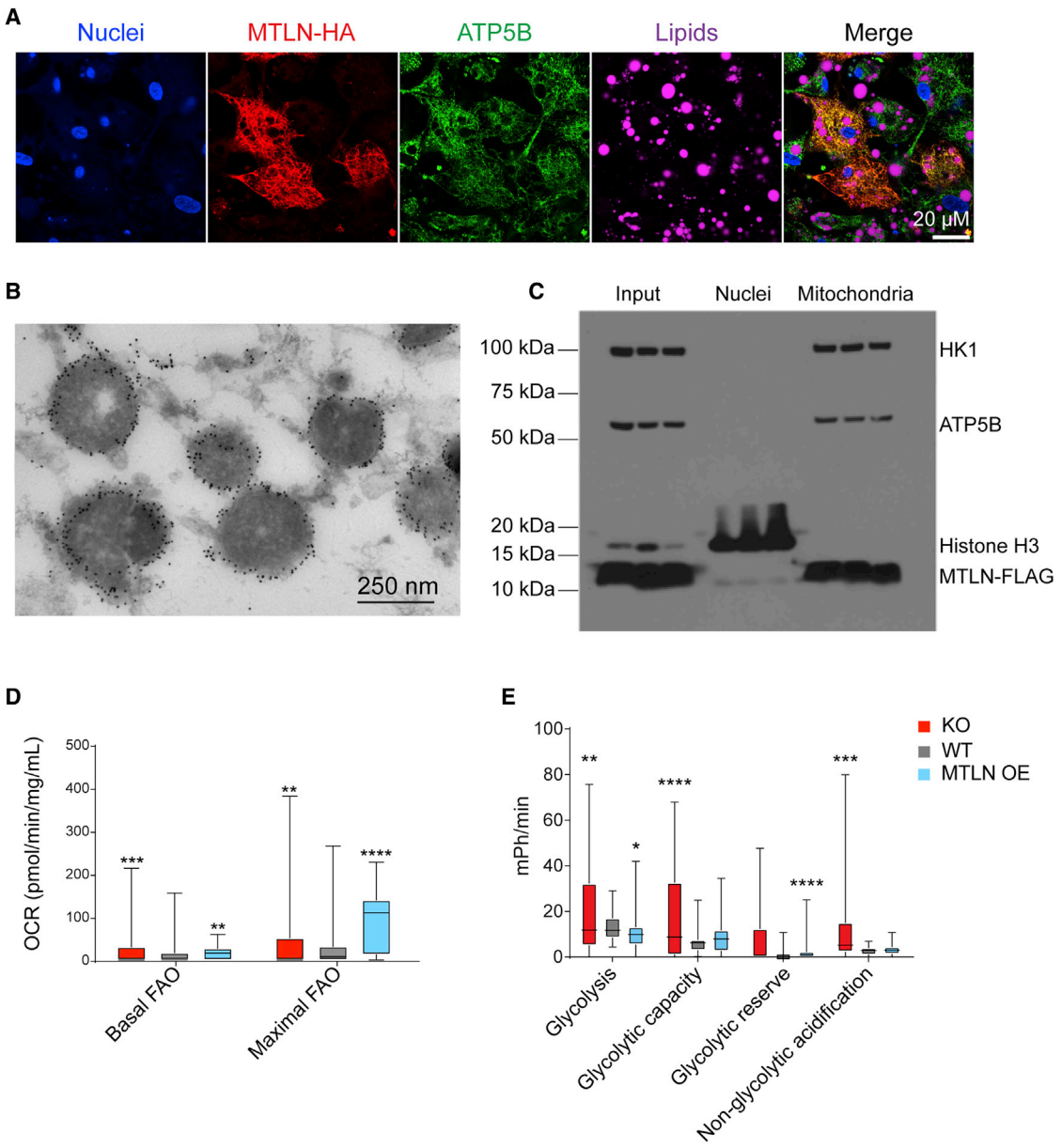


**Figure 3. *MTLN* Localizes to the Mitochondrion and Affects Energetics Regulation**

(A) Confocal microscopy showing *MTLN*-HA (red), ATP5B (green), neutral lipids (purple), and nuclei (blue) in differentiated hPSC-adipocytes. Scale bar, 20 μm.

(B) Immunogold labeling of *MTLN*-HA in differentiated hPSC-adipocytes.

(C) Subcellular fractionation of differentiated hPSC-adipocytes. Whole-cell lysate is blotted as input material.

(D) Basal and maximal fatty acid oxidation of hPSC-adipocytes. n = 35.

(E) Comparison of glycolysis, glycolytic capacity, and reserve in hPSC-adipocytes. n = 30. Bars represent mean values ±SD.

*p ≤ 0.05, **p ≤ 0.01, ***p ≤ 0.001, ****p ≤ 0.0001; two-way ANOVA. All n values are independent biological replicates. Related to Figure S3.

## DISCUSSION

Our experiments point toward the *MTLN* SEP of *LINC00116* as an important functional element in β-oxidation of fatty acids in human adipocytes. This situates *MTLN* among the rapidly expanding class of SEPs encoded by lncRNAs, supporting the hypothesis that there are many functional small peptides yet to be discovered. *MTLN* localizes to the mitochondria and affects energetics and lipid metabolism in human adipocytes, mice, and isolated

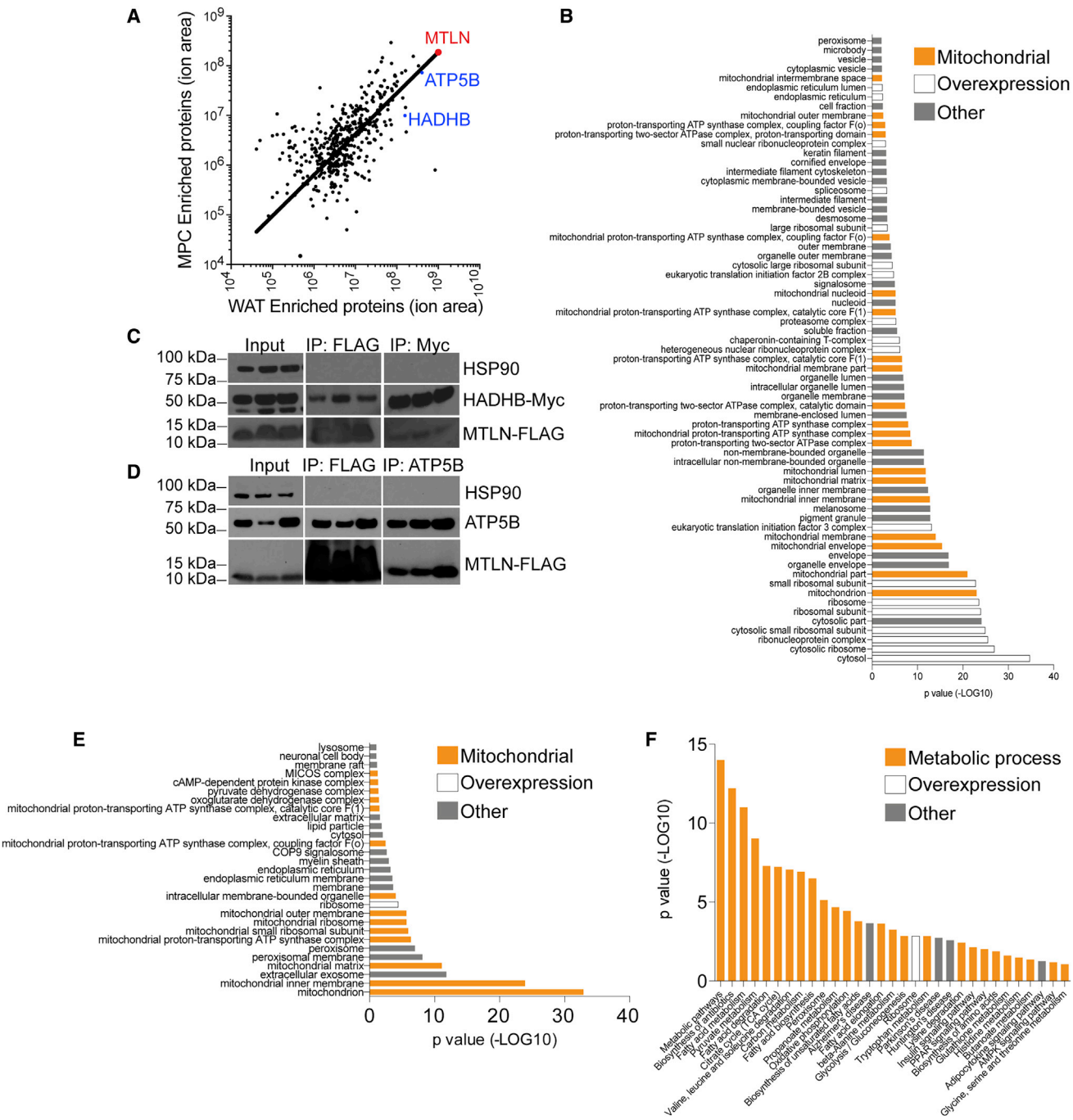


**Figure 4. *MTLN* Interacts with the Mitochondrial Energetics Machinery**

(A) Mass spectrometric profiling of co-immunoprecipitated proteins bound to *MTLN*-FLAG in undifferentiated MPCs and hPSC-adipocytes. Red, *MTLN*; blue, ATP5B and HADHB. Trendline represents the linear regression of these data using a non-linear model. Data based on two independent biological replicates each of MPCs and WAT. Data in Supplemental Table 2.

(B) DAVID gene ontology analysis of the cellular compartment categorization of co-immunoprecipitated proteins bound to *MTLN*-Flag. Orange, mitochondrial localization; white, protein translation machinery; gray, other. Modified Fisher exact p value, EASE score. Data in Supplemental Table 3.

(C) Immunoblot of HADHB co-immunoprecipitated with *MTLN*-FLAG. Whole-cell lysate is shown as input material.

(D) Immunoblot of ATP5B co-immunoprecipitated with *MTLN*-FLAG. Whole-cell lysate is shown as input material.

*(legend continued on next page)*

murine adipocytes. Interaction with HADHB and accumulation of TGs in *MTLN* KO hPSC-adipocytes implicates *MTLN* in long-chain fatty acid catabolism. HADHB catalyzes the final step in long-chain FAO, thought to be the rate-limiting step (Li and Schulz, 1988; Olowe and Schulz, 1982). Our data suggest *MTLN* augments the rate of β-oxidation of long-chain fatty acids, possibly through direct interaction with HADHB. It does so at the expense of other energy-producing pathways, including glycolysis and non-FAO mitochondrial respiration. In this model, decreased intracellular fatty acids would decrease feedback inhibition of lipolysis (Fain and Shepherd, 1975), resulting in the lipolytic phenotype observed in our *in vitro* systems. Ongoing research will determine the mechanism by which *MTLN* modulates the rate of β-oxidation, how the peptide is trafficked to the mitochondria, and how *MTLN* overexpression affects systemic phenotypes in mice.

Our data suggest that there is regulation of *MTLN*'s function through certain environmental conditions. *MTLN* does not have an effect on browning adipocytes from our data; therefore, we speculate it is not regulated by cold exposure. However, it appears that nutritional status has a profound effect on *MTLN*'s function. Our Seahorse data show that oxidative phosphorylation is specifically enhanced under nutrient starvation conditions, when the adipocytes are utilizing endogenous lipids for FAO. This phenomenon may be very interesting for further study into the fuel source preference of *MTLN* activity.

Aside from the endogenous expression, most of our experiments have been performed with tagged overexpression of *MTLN*. We were not able to generate an antibody to the endogenous peptide; hence, this was our only viable approach. It is hoped that future work can follow up on our data and confirm the peptide interactions using the endogenous *MTLN*.

The pool of undiscovered functional SEPs remains fertile ground for drug discovery and development. hPSCs are a perfect model to study the role of these novel genes in a human system as they are amenable to functional screening, genetic manipulation, as well as differentiation into any desired tissue to mechanistically understand a SEP's purpose. This study can serve as a blueprint for functional discovery of uncharacterized SEPs, of which there are now predicted to be a plethora.

The small size of SEPs lends them to repurposing as peptide therapies, particularly if they are secreted and function in an endocrine fashion to modulate systemic phenotypes (Lee et al., 2015). *MTLN*'s apparent function recommends its application as a gene therapy for clearance of excess lipids in adipose tissue. Obesity is on the rise in developed and developing countries, with 500 million cases worldwide (Malik et al., 2013). Gene therapies delivering *MTLN* to white adipose could combat this global trend, serving as a biological trigger for the catabolism of FFAs by β-oxidation. However, further research is warranted as care needs to be taken that this does not lead to the unfavorable metabolic state of deleterious increased plasma TG levels.

## EXPERIMENTAL PROCEDURES

### Mouse Models

All procedures used in animal experiments were in accordance and with approval from the pertinent Institutional Animal Care and Use Committees at Harvard University. *MTLN* KO mice were generated via CRISPR/Cas9 technology in the Genome Modification Facility at Harvard University. Both male and female *MTLN* global KO mice and WT littermates were used in this study. They were housed three to five mice per cage with free access to water and normal chow diet or HFD (60/FAT, TD.06414). Blood was collected from tail tips after 16-h fasting, and plasma was further isolated.

### Cell Lines

HUES9 embryonic stem cells were cultured as described previously (Cowan et al., 2004) in mTeSR growth medium (STEMCELL Technologies). Adipocyte differentiation of embryonic stem cells was performed as described previously (Lee and Cowan, 2014). Genome editing in the HUES9 cell line was performed following a published protocol (Peters et al., 2013) using the guide RNA and screening primer sequences in Supplemental Table 1. Cell lines were tested for mycoplasma contamination and were not contaminated during this study.

The SGBS cell line was a gift from Dr. Martin Wabitsch's lab and cultured as described previously (Wabitsch et al., 2001). Fully confluent SGBS cells were differentiated to adipocytes using adipogenic medium: DMEM (Corning) supplemented with 7.5% Knockout Serum Replacement, 1% penicillin/streptomycin, 0.5% non-essential amino acids, 1 μM dexamethasone, 10 μg/mL insulin, and 0.5 μM rosiglitazone for 21 days. To generate Cas9-positive SGBS cells, lentivirus was packaged using the Lenti-Cas9-Blast plasmid available Addgene. After application of lentivirus, Cas9-positive SGBS cells were selected using 10 μg/mL blasticidin for 5 days. Guide RNAs were cloned into the Lenti-Guide-Puro plasmid and lentivirus was packaged according to a

(E) DAVID gene ontology analysis of the cellular compartment categorization of co-immunoprecipitated proteins bound to *MTLN*-Flag in hPSC-adipocytes but not MPCs. Orange, mitochondrial localization; white, protein translation machinery; gray, other. Modified Fisher exact p value, EASE score.

(F) Gene ontology analysis describing the biological pathways enriched in the co-immunoprecipitated proteins bound to *MTLN*-Flag in hPSC-adipocytes but not in MPCs. Orange, mitochondrial processes; white, protein translation and overexpression; gray, other. Pathways and processes are colored through personal interpretation of DAVID terms. Modified Fisher exact p value, EASE score.

Related to Figure S4.

published protocol (Lee and Cowan, 2014). Three guide RNA lentiviruses were pooled and applied to SGBS-Cas9 cells. These cells were then selected with puromycin (2 μg/mL) for 4 days. Selected cells were then differentiated according to the above protocol.

## Isolation and Differentiation of Pre-adipocytes from Mouse White Adipose Tissue

Inguinal fat pads from 6- to 8-week-old mice were carefully dissected, cut into small pieces, and digested with 1 mg/mL collagenase A at 37°C for 45 min. The cell suspension was then filtered through a 100-μm cell strainer followed by centrifugation at 150 × *g* for 5 min. The cell pellet was resuspended with complete medium (DMEM/F12 with 10% fetal bovine serum [FBS], 1% penicillin/streptomycin) and plated in gelatin-coated 10-cm plates. For differentiation 50,000 cells were seeded per well of a 24-well plate. The next day, induction medium (complete medium with 1 μM dexamethasone, 5 μg/mL insulin, 0.5 mM IBMX, and 5 μM rosiglitazone) was added. On day 4, maintenance medium (complete medium with 1 μg/mL insulin and 5 μM rosiglitazone) was added and the cells further differentiated for 11 days before performing the assays.

## RNA Isolation, cDNA Synthesis, and qPCR

RNA was extracted from adherent cells using TRIzol reagent reagent according to the manufacturer's instructions (Thermo Scientific). cDNA synthesis was performed using qScript cDNA SuperMix according to the manufacturer's instructions (Quanta Biosciences). qPCR of *LINC00116*, *MTLN*, *UCP1*, *CPT1*, *RPLP0*, *1500011K16Rik*, and *RPL27* was performed using primer sets listed in Table 1 in conjunction with Fast SYBR Green Master Mix (Thermo Scientific). Expression data are presented after calculating the relative expression compared with the housekeeping gene *RPLP0* or *Rpl27*, using the equation relative quantification (RQ) = 100/(2^(Target Gene Ct – *RPLP0* Ct)).

## Immunofluorescence

Cells were washed in phosphate-buffered saline (PBS) and then fixed in ice-cold methanol at −20°C for 15 min. Cells were then washed three times with PBS, and blocked for 1 h at room temperature with 5% (w/v) bovine serum albumin (BSA), Fraction V (Millipore), 0.1% Triton X-100 (Sigma) in PBS. Primary antibodies were incubated overnight at 4°C. Cells were then washed three times in PBS, and incubated with secondary antibodies conjugated to fluorophores for 1 h at room temperature. Nuclei were labeled with Hoechst (Thermo Scientific) and neutral lipids were stained with the LipidTOX Red or LipidTOX Deep Red (Thermo Scientific) fluorescent dye for 30 min at room temperature. Antibodies and dyes with working dilutions are listed in Table 1.

## TG Quantification

Cells were washed in PBS, scraped in PBS supplemented with 5% Nonidet P40 Substitute (Sigma). Cells were lysed by two 30-s cycles of sonication on high power using a BioRuptor sonicator (Diagenode). Debris was pelleted at 14,000 × *g* for 10 min at 4°C, then soluble protein concentration was measured using the bicinchoninic acid assay following the manufacturer's instructions (Thermo Scientific). In both a commercial standard (Abcam) and experimental samples, TGs were solubilized by two cycles of heating to 95°C for 2 min followed by vortexing. TG concentrations were measured using the Infinity Triglycerides Reagent (Thermo Scientific) as per the manufacturer's instructions. Concentrations were normalized to protein concentration and differentiation efficiency, and plotted as TGs/adipocyte.

## Lipolysis Assay

Differentiated adipocytes were starved for 4 h in serum-free no-glucose DMEM, and treated with or without forskolin for an additional 4 h at 37°C. Medium was collected, and cells were harvested as described above for quantification of TG content. Concentration of FFAs and glycerol in conditioned medium was quantified using the Lipolysis Assay Kit (ZenBio, Durham, NC) according to the manufacturer's instructions. Concentrations were normalized to TG and protein concentration of whole-cell lysate and differentiation efficiency, and plotted as FFA release/adipocyte or glycerol release/adipocyte.

## Expression Plasmid Construction

The evolutionarily conserved *MTLN* peptide sequence was downloaded from NCBI and synthesized *in vitro* (Eurofins Genomics) for cloning with a multi-site gateway cloning strategy (Thermo Scientific). A lentiviral packaging vector, a donor plasmid carrying the EF1 alpha promoter, and a donor plasmid carrying the *MTLN* peptide tagged with a C-terminal 3× FLAG or 3× HA peptide were recombined in a three-way cloning reaction.

## Cell Fractionation

Nuclei were isolated from five million cells using a 2% Nonidet P40 Substitute (Sigma Aldrich) solution, otherwise following a published protocol (Nabbi and Riabowol, 2015). Mitochondria were then pelleted by centrifugation at 17,000 × *g* for 15 min at 4°C.

## Western Blotting

Bis-Tris polyacrylamide gels (4%–12%) were run using LDS sample buffer with MOPS running buffer (Thermo Scientific). Cells were lysed using RIPA buffer, cell debris was pelleted at 14,000 × *g*, and soluble protein concentrations were measured as described above. Protein samples were supplemented with a final concentration of 5 mM dithiothreitol before heating at 95°C for 5 min. After polyacrylamide gel electrophoresis using a Mini-Cell apparatus (Thermo Scientific), proteins were transferred to a nitrocellulose membrane in transfer buffer (25 mM Tris, 192 mM glycine, 10% methanol) for 1 h by applying 100 V of constant voltage at 4°C. Primary and secondary antibodies and working dilutions are detailed in Table 1.

## Transmission Electron Microscopy

*MTLN* OE or WT hPSC-adipocytes were detached from the dish with a cell scraper. The cell suspension was layered on top of a 200-μL cushion of 4% paraformaldehyde (PFA)/0.1% glutaraldehyde (in 0.1 M sodium phosphate buffer [pH 7.4]) in an Eppendorf tube and pelleted for 3 min at 3,000 rpm. The supernatant was removed carefully, fresh 4% PFA/0.1% glutaraldehyde mixture was added without resuspending the pellet. After 2 h of fixation at room temperature the fixative was replaced with PBS without disturbing the pellet. PBS then was replaced with 2.3 M sucrose

in PBS (containing 0.2 M glycine to quench free aldehyde groups) for 15 min. The pellet then was flash frozen in liquid nitrogen. Samples were sectioned at −120°C, and the sections were transferred to formvar- and carbon-coated copper grids. Grids were floated on PBS until immunogold labeling was carried out. Gold labeling was carried out at room temperature on a piece of parafilm. All antibodies and protein A-gold were diluted in 1% BSA. The diluted antibody solution was centrifuged for 1 min at 14,000 rpm before labeling to avoid possible aggregates. Grids were floated on drops of 1% BSA in PBS for 10 min to block for non-specific labeling, transferred to 5-μL drops of primary antibody, and incubated for 30 min. The grids were then washed in 4 drops of PBS for a total of 15 min, transferred to 5 μL drops of protein A-gold for 20 min, washed in 4 drops of PBS for 15 min and 6 drops of double distilled water. Contrasting/embedding of the labeled grids was carried out on ice in 0.3% uranyl acetete in 2% methyl cellulose for 10 min. Grids were picked up and the excess liquid was removed by streaking on filter paper (Whatman grade 1), leaving a thin coat of methyl cellulose. The grids were examined in a JEOL 1200EX and images were recorded with an AMT 2k CCD camera.

## Extracellular Flux Analysis

A Seahorse XF24 Analyzer (Seahorse Bioscience) was used to assess oxygen consumption and extracellular acidification rates. MPCs (40,000) were plated in each well 2 days before induction of adipogenesis by the above protocol. The mitochondrial stress test, glycolysis stress test, and the XF Palmitate-BSA FAO Substrate kits were used according to the manufacturer's protocol. Carbonyl cyanide m-chlorophenylhydrazone was used at 0.5 μM final concentration in the mitochondrial stress test, and at 2 μM final concentration in the FAO assay. Rate measurement cycles consisted of 2 min of mixing, 1 min of waiting, and 5 min of measurement.

## Co-immunoprecipitation

Differentiated adipocytes were lysed in Pierce IP Buffer (Thermo Scientific) supplemented with protease and phosphatase inhibitors (Roche Life Science). Cell debris was pelleted at 20,000 × *g* for 15 min at 4°C. After removal of the lipid supernatant, 10 mg of protein from the infranatant was incubated overnight on an end-over-end rotator at 4°C with antibodies directed against the FLAG-tag (conjugated to magnetic beads, Sigma Aldrich, 20 μL of packed gel volume), ATP synthase, beta subunit (10 μg, Abcam, ab128743), or the C-terminal Myc tag of HADHB (10 μg, Abcam, ab9106) (Table 1). Pre-immune immunoglobulin immunoprecipitations (IPs) were performed as controls with equal quantities of protein, using magnetic bead-conjugated mouse immunoglobulin G (IgG) (Cell Signaling Technology) or rabbit IgG (Santa Cruz). After overnight incubation, ATP synthase and HADHB IP reactions and rabbit IgG control reactions were incubated with protein A-conjugated magnetic beads (25 μL, Thermo Scientific) for 1 h at room temperature on an end-over-end rotator. Bead-protein complexes were pelleted on a magnetic stand and washed with Tris-buffered saline ten times. Protein was eluted from the beads using 100 μL of 0.1 M glycine (pH 3.0). Samples were equilibrated to neutral pH by addition of 1 M triethylammonium bicarbonate (TEAB) buffer (pH 8.0) to a final concentration of 100 mM TEAB.

## Co-immunoprecipitation Proteomics

Each sample was submitted for a single liquid chromatography-tandem mass spectrometry experiment that was performed on an LTQ Orbitrap Elite (Thermo Fischer) equipped with a Waters nanoACQUITY HPLC pump. Peptides were separated onto a 100-μm inner diameter microcapillary trapping column packed first with approximately 5 cm of C18 ReproSil resin (5 μm, 100 Å, Dr. Maisch, Germany) followed by an analytical column ~20 cm of ReproSil resin (1.9 μm, 200 Å, Dr. Maisch). Separation was achieved by applying a gradient from 5% to 27% acetonitrile in 0.1% formic acid over 90 min at 200 nL $min^{-1}$. Electrospray ionization was enabled by applying a voltage of 1.8 kV using a homemade electrode junction at the end of the microcapillary column and sprayed from fused silica pico tips (New Objective). The LTQ Orbitrap Elite was operated in the data-dependent mode for the mass spectrometry methods. The mass spectrometry survey scan was performed in the Orbitrap in the range of 395–1,800 m/z at a resolution of $6 \times 10^4$, followed by the selection of the 20 most intense ions (TOP20) for collision-induced dissociation (CID)-tandem mass spectrometry fragmentation in the ion trap using a precursor isolation width window of 2 m/z, automatic gain control (AGC) setting of 10,000, and a maximum ion accumulation of 200 ms. Singly charged ion species were not subjected to CID fragmentation. Normalized collision energy was set to 35 V and an activation time of 10 ms, AGC was set to 50,000, and the maximum ion time was 200 ms. Ions in a 10-ppm m/z window around ions selected for tandem mass spectrometry were excluded from further selection for fragmentation for 60 s.

## Statistical Analysis of qPCR, Mouse Cohort, Differentiation Efficiency, TG Assay, Lipolysis Assay, and Extracellular Flux Analyzer Data

Prism 5 (GraphPad) was used to create charts and perform statistical analyses in all figures. Student's t test (paired), one- (three-group) or two-way ANOVA (three or more groups, multiple conditions) was used to compare KO and OE genotypes or treatment conditions to the WT group.

## Gene Ontology Analyses

Co-immunoprecipitated proteins were analyzed using DAVID (Huang da et al., 2009). Ion area values of background control IP samples were subtracted from *MTLN*-Flag IP sample values to determine *MTLN*-Flag-specific enrichment of protein interactants.

## Analysis of Proteomics Data

Raw data were submitted for analysis in Proteome Discoverer 2.1.0.81 (Thermo Scientific) software. Assignment of tandem mass spectrometry spectra was performed using the Sequest HT algorithm by searching the data against a protein sequence database, including all entries from the Human UniProt database (SwissProt 16,768 and TrEMBL 62,460 [total of 79,228 protein forms], 2015) and other known contaminants, such as human keratins and common lab contaminants. Sequest HT searches were performed using a 20-ppm precursor ion tolerance and requiring each peptide N/C terminus to adhere with trypsin protease specificity while allowing up to two missed cleavages. Cysteine carbamidomethyl (+57.021) was set as static modification while methionine oxidation

(+15.99492 Da) was set as variable modification. Tandem mass spectrometry spectra assignment false discovery rate of 1% on protein level was achieved by applying the target-decoy database search. Filtering was performed using a Percolator (64 bit version, reference 6). For quantification, a 0.02-m/z window centered on the theoretical m/z value of each the six reporter ions and the intensity of the signal closest to the theoretical m/z value was recorded. Reporter ion intensities were exported in result files of Proteome Discoverer 2.1 searches as Excel tables. All fold changes were analyzed after normalization between samples based on total unique peptide ion signals.

## SUPPLEMENTAL INFORMATION

Supplemental Information can be found online at https://doi.org/10.1016/j.stemcr.2020.03.002.

## AUTHOR CONTRIBUTIONS

Manuscript Preparation, M.F. and C.R.W.; Study Supervision, C.A.C.; Study Support, J.L.R. and C.A.C.; smORF Conservation, L.A.G. and J.L.R.; Human PSC and Mouse Genome Editing, Q.D.; Mass Spectrometry, M.H.C.F. and C.R.W.; Mouse Experiments, H.Y. and T.T.; Murine Pre-adipocyte Characterization, M.F., H.Y., and T.T.; Human Adipocyte Characterization, M.F. and C.R.W.; SGBS Pre-adipocyte Characterization, M.F. and H.Y.; smORF Localization, M.F. and C.R.W.; Metabolic Assays, M.F.; Expression and Proteomics Analysis, M.F.; Supporting Experiments, M.H.C.F., C.S., and B.D.P. All authors approved the results and manuscript.

## ACKNOWLEDGMENTS

The authors thank the Harvard University Mass Spectrometry and Proteomics Resource Laboratory for their assistance with proteomics analyses. Thanks to Maria Ericsson and the Harvard Medical School Electron Microscopy core for performing immunogold experiments. Thanks to Feng Zhang for providing us with the Lenti-Cas9-Blast and LentiGuide-Puro plasmids. This study was funded by NIH/NIDDK R01DK097768-01, NIH/NIDDK RO1DK095384, and NIH/NHLBI U01HL107440.

Received: August 20, 2019
Revised: February 29, 2020
Accepted: March 2, 2020
Published: April 2, 2020

## REFERENCES

Anderson, D.M., Anderson, K.M., Chang, C.L., Makarewich, C.A., Nelson, B.R., McAnally, J.R., Kasaragod, P., Shelton, J.M., Liou, J., Bassel-Duby, R., et al. (2015). A micropeptide encoded by a putative long noncoding RNA regulates muscle performance. Cell *160*, 595–606.

Cabili, M.N., Trapnell, C., Goff, L., Koziol, M., Tazon-Vega, B., Regev, A., and Rinn, J.L. (2011). Integrative annotation of human large intergenic noncoding RNAs reveals global properties and specific subclasses. Genes Dev. *25*, 1915–1927.

Chugunova, A., Loseva, E., Mazin, P., Mitina, A., Navalayeu, T., Bilan, D., Vishnyakova, P., Marey, M., Golovina, A., Serebryakova, M., et al. (2019). LINC00116 codes for a mitochondrial peptide linking respiration and lipid metabolism. Proc. Natl. Acad. Sci. U S A *116*, 4940–4945.

Collins, F.S., and Mansoura, M.K. (2001). The Human Genome Project. Revealing the shared inheritance of all humankind. Cancer *91*, 221–225.

Cowan, C.A., Klimanskaya, I., McMahon, J., Atienza, J., Witmyer, J., Zucker, J.P., Wang, S., Morton, C.C., McMahon, A.P., Powers, D., et al. (2004). Derivation of embryonic stem-cell lines from human blastocysts. N. Engl. J. Med. *350*, 1353–1356.

D'Lima, N.G., Ma, J., Winkler, L., Chu, Q., Loh, K.H., Corpuz, E.O., Budnik, B.A., Lykke-Andersen, J., Saghatelian, A., and Slavoff, S.A. (2017). A human microprotein that interacts with the mRNA decapping complex. Nat. Chem. Biol. *13*, 174–180.

Fain, J.N., and Shepherd, R.E. (1975). Free fatty acids as feedback regulators of adenylate cyclase and cyclic 3′:5′-AMP accumulation in rat fat cells. J. Biol. Chem. *250*, 6586–6592.

Guttman, M., and Rinn, J.L. (2012). Modular regulatory principles of large non-coding RNAs. Nature *482*, 339–346.

Huang da, W., Sherman, B.T., and Lempicki, R.A. (2009). Systematic and integrative analysis of large gene lists using DAVID bioinformatics resources. Nat. Protoc. *4*, 44–57.

Lee, C., Zeng, J., Drew, B.G., Sallam, T., Martin-Montalvo, A., Wan, J., Kim, S.J., Mehta, H., Hevener, A.L., de Cabo, R., et al. (2015). The mitochondrial-derived peptide MOTS-c promotes metabolic homeostasis and reduces obesity and insulin resistance. Cell Metab. *21*, 443–454.

Lee, Y.K., and Cowan, C.A. (2014). Differentiation of white and brown adipocytes from human pluripotent stem cells. Methods Enzymol. *538*, 35–47.

Li, J.X., and Schulz, H. (1988). 4-Bromo-2-octenoic acid specifically inactivates 3-ketoacyl-CoA thiolase and thereby fatty acid oxidation in rat liver mitochondria. Biochemistry *27*, 5995–6000.

Lin, M.F., Jungreis, I., and Kellis, M. (2011). PhyloCSF: a comparative genomics method to distinguish protein coding and non-coding regions. Bioinformatics *27*, i275–282.

Lin, Y.F., Xiao, M.H., Chen, H.X., Meng, Y., Zhao, N., Yang, L., Tang, H., Wang, J.L., Liu, X., Zhu, Y., et al. (2019). A novel mitochondrial micropeptide MPM enhances mitochondrial respiratory activity and promotes myogenic differentiation. Cell Death Dis. *10*, 528.

Makarewich, C.A., Baskin, K.K., Munir, A.Z., Bezprozvannaya, S., Sharma, G., Khemtong, C., Shah, A.M., McAnally, J.R., Malloy, C.R., Szweda, L.I., et al. (2018). MOXI is a mitochondrial micropeptide that enhances fatty acid beta-oxidation. Cell Rep. *23*, 3701–3709.

Malik, V.S., Willett, W.C., and Hu, F.B. (2013). Global obesity: trends, risk factors and policy implications. Nat. Rev. Endocrinol. *9*, 13–27.

Matsumoto, A., Pasut, A., Matsumoto, M., Yamashita, R., Fung, J., Monteleone, E., Saghatelian, A., Nakayama, K.I., Clohessy, J.G., and Pandolfi, P.P. (2017). mTORC1 and muscle regeneration are regulated by the LINC00961-encoded SPAR polypeptide. Nature *541*, 228–232.

Moisan, A., Lee, Y.K., Zhang, J.D., Hudak, C.S., Meyer, C.A., Prummer, M., Zoffmann, S., Truong, H.H., Ebeling, M., Kiialainen, A., et al. (2015). White-to-brown metabolic conversion of human adipocytes by JAK inhibition. Nat. Cell Biol. *17*, 57–67.

Nabbi, A., and Riabowol, K. (2015). Rapid isolation of nuclei from cells in vitro. Cold Spring Harb. Protoc. *2015*, 769–772.

Olowe, Y., and Schulz, H. (1982). 4-Bromocrotonic acid, an effective inhibitor of fatty acid oxidation and ketone body degradation in rat heart mitochondria. On the rate-determining step of beta-oxidation and ketone body degradation in heart. J. Biol. Chem. *257*, 5408–5413.

Peters, D.T., Cowan, C.A., and Musunuru, K. (2013). Genome editing in human pluripotent stem cells. In StemBook, L. Girard, ed. (Harvard Stem Cell Institute) https://doi.org/10.3824/stembook.1.94.1.

Pope, B.D., Warren, C.R., Parker, K.K., and Cowan, C.A. (2016). Microenvironmental control of adipocyte fate and function. Trends Cell Biol. *26*, 745–755.

Roberts, L.D., Bostrom, P., O'Sullivan, J.F., Schinzel, R.T., Lewis, G.D., Dejam, A., Lee, Y.K., Palma, M.J., Calhoun, S., Georgiadi, A., et al. (2014). beta-Aminoisobutyric acid induces browning of white fat and hepatic beta-oxidation and is inversely correlated with cardiometabolic risk factors. Cell Metab. *19*, 96–108.

Slavoff, S.A., Mitchell, A.J., Schwaid, A.G., Cabili, M.N., Ma, J., Levin, J.Z., Karger, A.D., Budnik, B.A., Rinn, J.L., and Saghatelian, A. (2013). Peptidomic discovery of short open reading frame-encoded peptides in human cells. Nat. Chem. Biol. *9*, 59–64.

Stein, C.S., Jadiya, P., Zhang, X., McLendon, J.M., Abouassaly, G.M., Witmer, N.H., Anderson, E.J., Elrod, J.W., and Boudreau, R.L. (2018). Mitoregulin: a lncRNA-encoded microprotein that supports mitochondrial supercomplexes and respiratory efficiency. Cell Rep. *23*, 3710–3720.e8.

Sun, L., Goff, L.A., Trapnell, C., Alexander, R., Lo, K.A., Hacisuleyman, E., Sauvageau, M., Tazon-Vega, B., Kelley, D.R., Hendrickson, D.G., et al. (2013). Long noncoding RNAs regulate adipogenesis. Proc. Natl. Acad. Sci. U S A *110*, 3387–3392.

Venter, J.C., Adams, M.D., Myers, E.W., Li, P.W., Mural, R.J., Sutton, G.G., Smith, H.O., Yandell, M., Evans, C.A., Holt, R.A., et al. (2001). The sequence of the human genome. Science *291*, 1304–1351.

Wabitsch, M., Brenner, R.E., Melzner, I., Braun, M., Moller, P., Heinze, E., Debatin, K.M., and Hauner, H. (2001). Characterization of a human preadipocyte cell strain with high capacity for adipose differentiation. Int. J. Obes. Relat. Metab. Disord. *25*, 8–15.

**Stem Cell Reports, Volume *14***

## Supplemental Information

# Mitoregulin Controls β-Oxidation in Human and Mouse Adipocytes

**Max Friesen, Curtis R. Warren, Haojie Yu, Takafumi Toyohara, Qiurong Ding, Mary H.C. Florido, Carolyn Sayre, Benjamin D. Pope, Loyal A. Goff, John L. Rinn, and Chad A. Cowan**

Figure S1

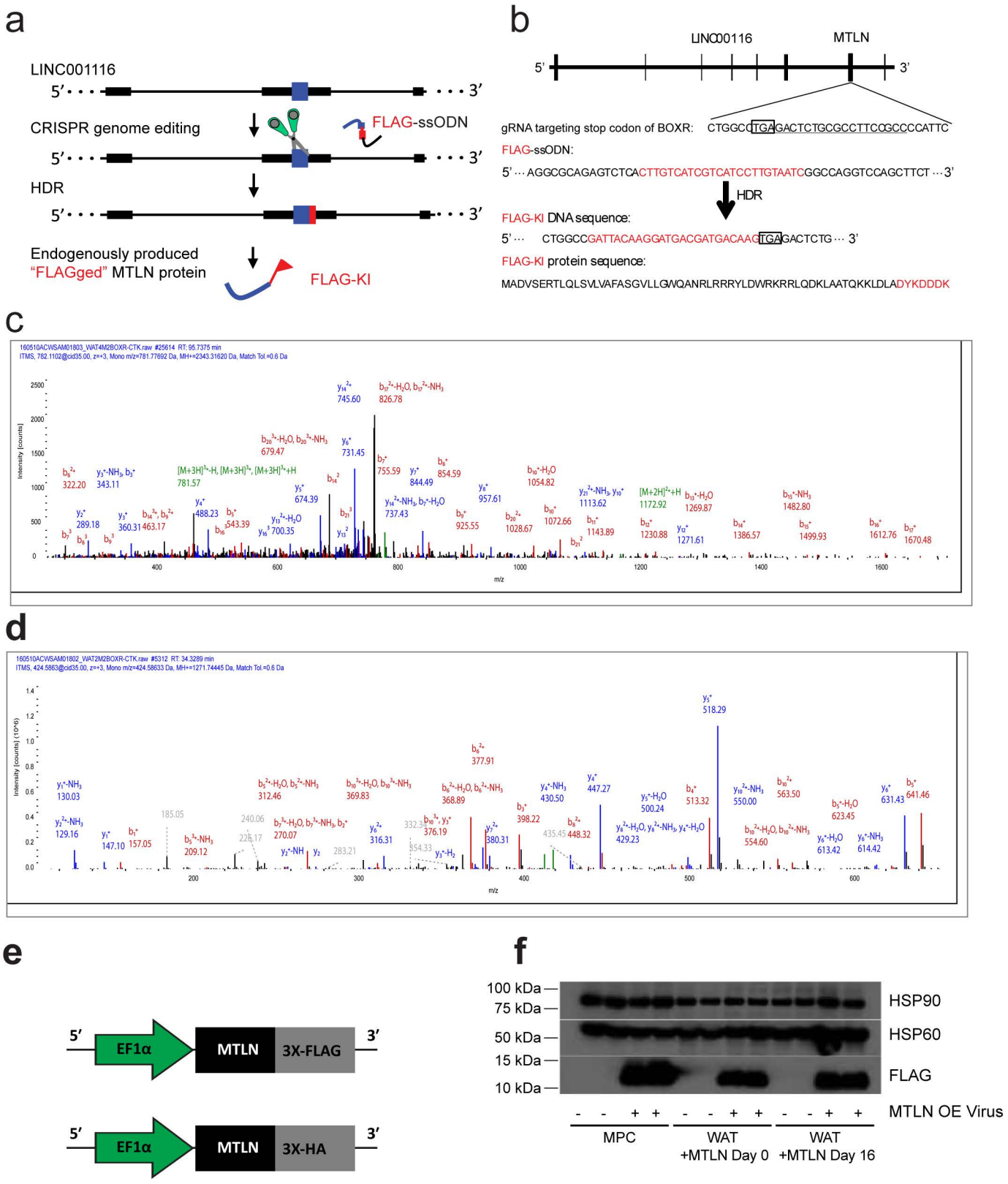
a
LINC001116
5′ · · · 3′
CRISPR genome editing
FLAG-ssODN
5′ · · · 3′
HDR
5′ · · · 3′
Endogenously produced
"FLAGged" MTLN protein
FLAG-KI
b
LINC00116
MTLN
5′
3′
gRNA targeting stop codon of BOXR: CTGGCCTGAGACTCTGCGCCTTCCGCCCCATTC
FLAG-ssODN:
5′ ··· AGGCGCAGAGTCTCACTTGTCATCGTCATCCTTGTAATCGGCCAGGTCCAGCTTCT ··· 3′
HDR
FLAG-KI DNA sequence:
5′ ··· CTGGCCGATTACAAGGATGACGATGACAAGTGAGACTCTG ··· 3′
FLAG-KI protein sequence:
MADVSERTLQLSVLVAFASGVLLGWQANRLRRRYLDWRKRRLQDKLAATQKKLDLADYKDDDK
c
160510ACWSAM01803_WAT4M2BOXR-CTK.raw #25614 RT: 95.7375 min
ITMS, 782.1102@cid35.00, z=+3, Mono m/z=781.77692 Da, MH+=2343.31620 Da, Match Tol.=0.6 Da
Intensity [counts]
m/z
d
160510ACWSAM01802_WAT2M2BOXR-CTK.raw #5312 RT: 34.3289 min
ITMS, 424.5863@cid35.00, z=+3, Mono m/z=424.58633 Da, MH+=1271.74445 Da, Match Tol.=0.6 Da
Intensity [counts] (10^6)
m/z
e
5′
EF1α
MTLN
3X-FLAG
3′
5′
EF1α
MTLN
3X-HA
3′
f
100 kDa
75 kDa
50 kDa
15 kDa
10 kDa
HSP90
HSP60
FLAG
- - + + - - + + - - + +
MTLN OE Virus
MPC
WAT
+MTLN Day 0
WAT
+MTLN Day 16

Figure S2

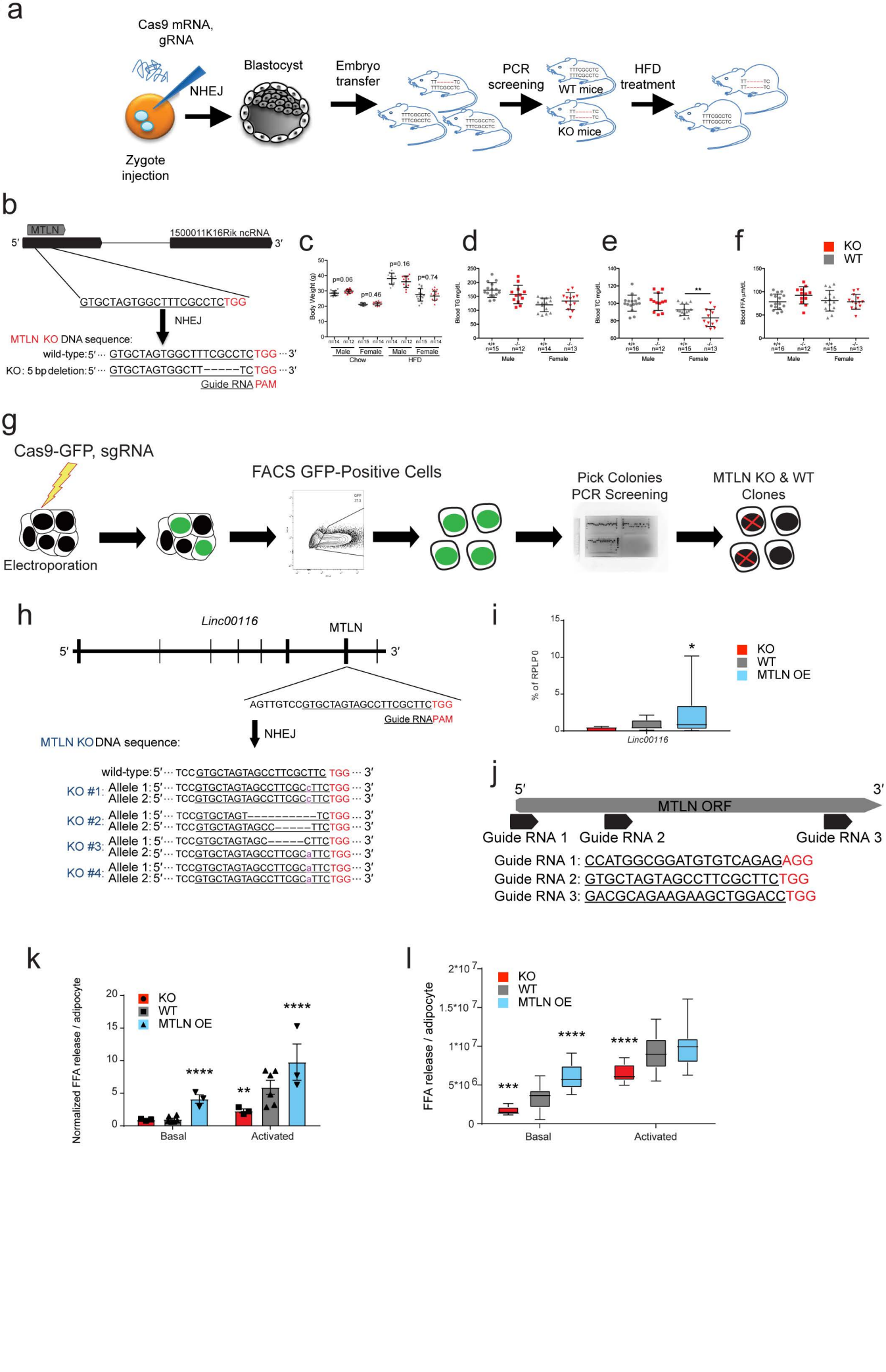
a
Cas9 mRNA, gRNA
NHEJ
Blastocyst
Zygote injection
Embryo transfer
PCR screening
WT mice
KO mice
HFD treatment
b
MTLN
1500011K16Rik ncRNA
5′
3′
GTGCTAGTGGCTTTCGCCTCTGG
NHEJ
MTLN KO DNA sequence:
wild-type: 5′··· GTGCTAGTGGCTTTCGCCTCTGG ··· 3′
KO: 5 bp deletion: 5′··· GTGCTAGTGGCTT−−−−−TCTGG ··· 3′
Guide RNA PAM
c
Body Weight (g)
p=0.06
p=0.46
p=0.16
p=0.74
Male Female Male Female
Chow HFD
d
Blood TG mg/dL
Male Female
e
Blood TC mg/dL
Male Female
f
KO
WT
Blood FFA μm/dL
Male Female
g
Cas9-GFP, sgRNA
Electroporation
FACS GFP-Positive Cells
Pick Colonies PCR Screening
MTLN KO & WT Clones
h
Linc00116
MTLN
5′
3′
AGTTGTCCGTGCTAGTAGCCTTCGCTTCTGG
Guide RNAPAM
NHEJ
MTLN KO DNA sequence:
wild-type: 5′··· TCCGTGCTAGTAGCCTTCGCTTC TGG ··· 3′
KO #1: Allele 1: 5′··· TCCGTGCTAGTAGCCTTCGCcTTCTGG ··· 3′
Allele 2: 5′··· TCCGTGCTAGTAGCCTTCGCcTTCTGG ··· 3′
KO #2: Allele 1: 5′··· TCCGTGCTAGT−−−−−−−−−TCTGG ··· 3′
Allele 2: 5′··· TCCGTGCTAGTAGCC−−−−−TTCTGG ··· 3′
KO #3: Allele 1: 5′··· TCCGTGCTAGTAGC−−−−−CTTCTGG ··· 3′
Allele 2: 5′··· TCCGTGCTAGTAGCCTTCGCaTTCTGG ··· 3′
KO #4: Allele 1: 5′··· TCCGTGCTAGTAGCCTTCGCaTTCTGG ··· 3′
Allele 2: 5′··· TCCGTGCTAGTAGCCTTCGCaTTCTGG ··· 3′
i
% of RPLP0
Linc00116
KO
WT
MTLN OE
j
5′
3′
MTLN ORF
Guide RNA 1
Guide RNA 2
Guide RNA 3
Guide RNA 1: CCATGGCGGATGTGTCAGAGAGG
Guide RNA 2: GTGCTAGTAGCCTTCGCTTCTGG
Guide RNA 3: GACGCAGAAGAAGCTGGACCTGG
k
Normalized FFA release / adipocyte
KO
WT
MTLN OE
Basal
Activated
l
FFA release / adipocyte
KO
WT
MTLN OE
Basal
Activated

Figure S3

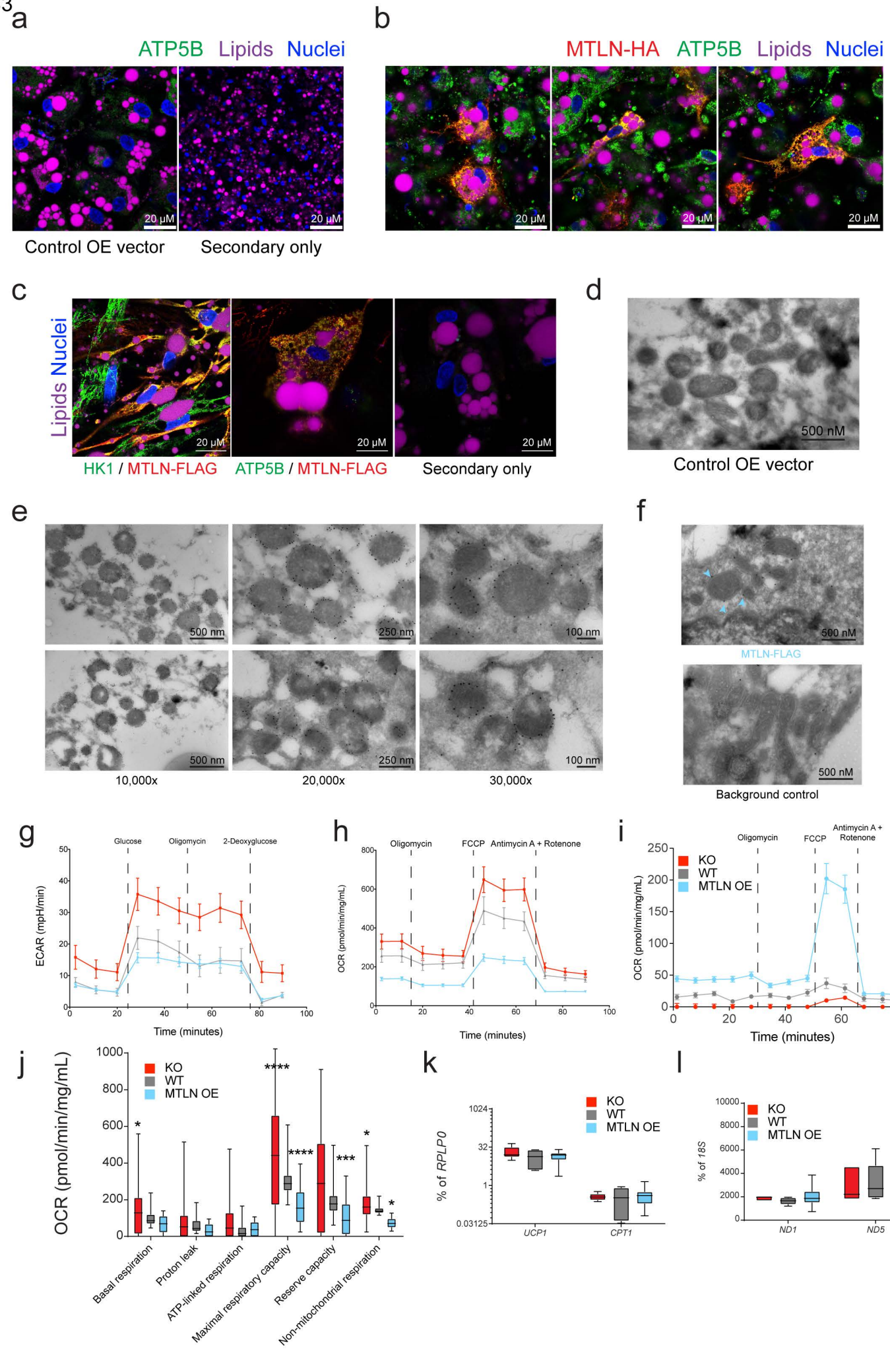
a
ATP5B Lipids Nuclei
20 μM
Control OE vector
Secondary only
b
MTLN-HA ATP5B Lipids Nuclei
c
Lipids Nuclei
HK1 / MTLN-FLAG
ATP5B / MTLN-FLAG
Secondary only
d
500 nM
Control OE vector
e
500 nm
250 nm
100 nm
10,000x
20,000x
30,000x
f
MTLN-FLAG
Background control
g
Glucose
Oligomycin
2-Deoxyglucose
ECAR (mpH/min)
Time (minutes)
h
Oligomycin
FCCP
Antimycin A + Rotenone
OCR (pmol/min/mg/mL)
Time (minutes)
i
KO
WT
MTLN OE
Time (minutes)
j
OCR (pmol/min/mg/mL)
Basal respiration
Proton leak
ATP-linked respiration
Maximal respiratory capacity
Reserve capacity
Non-mitochondrial respiration
k
% of RPLP0
UCP1
CPT1
l
% of 18S
ND1
ND5

Figure S4

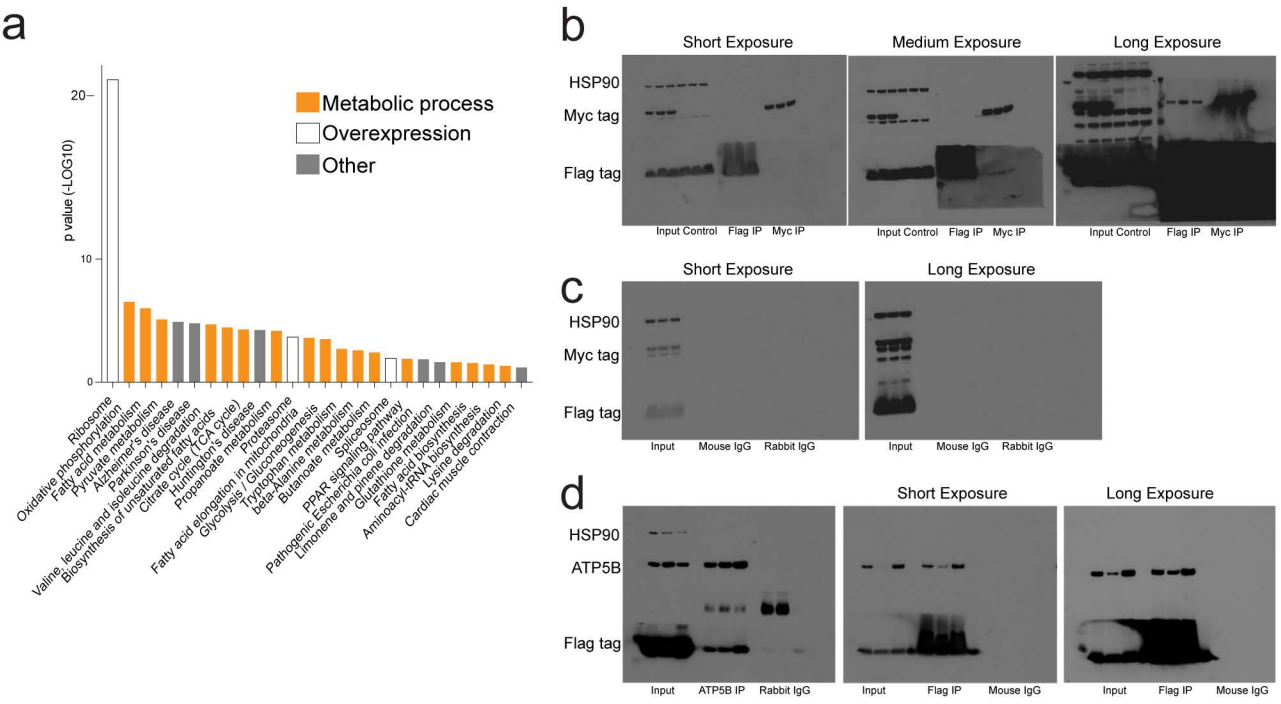
a
Metabolic process
Overexpression
Other
p value (-LOG10)
20
10
0
Ribosome
Oxidative phosphorylation
Fatty acid metabolism
Pyruvate metabolism
Alzheimer's disease
Parkinson's disease
Valine, leucine and isoleucine degradation
Biosynthesis of unsaturated fatty acids
Citrate cycle (TCA cycle)
Huntington's disease
Propanoate metabolism
Proteasome
Fatty acid elongation in mitochondria
Gluconeogenesis
Glycolysis / Gluconeogenesis
Tryptophan metabolism
beta-Alanine metabolism
Butanoate metabolism
Spliceosome
PPAR signaling pathway
Pathogenic Escherichia coli infection
Limonene and pinene degradation
Glutathione metabolism
Fatty acid degradation
Fatty acid biosynthesis
Aminoacyl-tRNA biosynthesis
Lysine degradation
Cardiac muscle contraction
b
Short Exposure
Medium Exposure
Long Exposure
HSP90
Myc tag
Flag tag
Input Control
Flag IP
Myc IP
c
Short Exposure
Long Exposure
HSP90
Myc tag
Flag tag
Input
Mouse IgG
Rabbit IgG
d
Short Exposure
Long Exposure
HSP90
ATP5B
Flag tag
Input
ATP5B IP
Rabbit IgG
Flag IP
Mouse IgG

**Supplemental Figure 1. MTLN-Flag methodology, related to Figure 1.** a) Schematic of the experimental procedure for knocking in a FLAG-tag at the c-terminus of MTLN in hPSCs. b) Partial sequence of the MTLN smORF, FLAG knock-in ssODN, and guide RNA used to generate knock-ins. The resultant DNA and peptide sequence after genome editing is also shown. c) Mass spectrometry spectrum identifying the 2.34 kDa peptide of MTLN. d) Mass spectrometry spectrum identifying the 1.27 kDa peptide of MTLN. e) Schematic of the MTLN-FLAG and MTLN-HA expression constructs inserted into a lentiviral packaging vector. f) Immunoblot demonstrating overexpression of lentiviral MTLN-FLAG in MPCs, MPCs differentiated into hPSC-adipocytes (WAT), or hPSC-adipocytes transduced with MTLN-FLAG after differentiation (WAT+MTLN Day 16).

**Supplemental Figure 2. Supplemental data describing mouse and *in vitro* models of MTLN function, related to Figure 2.** a) Experimental design for the creation of $MTLN^{-/-}$ mice and HFD treatment. b) Schematic of the murine *1500011K16Rik* ncRNA gene and MTLN smORF. The guide RNA is underlined, the protospacer-adjacent motif (PAM) is in red. Knockout mutation sequence indicated below. c) Body weight of mice on chow or HFD (10.5 weeks). d-f) Serum concentrations of TG (d), total cholesterol (e), and FFA (f) on chow diet. g) Experimental design for knocking out MTLN in hPSCs. h) Schematic of the human *LINC00116* gene and MTLN smORF. The guide RNA is underlined, the PAM is in red. Knockout line indel sequences indicated below. i) qRT-PCR analysis of *MTLN* expression in differentiated hPSC-adipocytes. n=18 for WT, 30 for KO, 48 for OE. j) Pool of guide RNA sequences used in SGBS knockout experiments. k) Concentration of FFAs released into the medium of differentiated murine pre-adipocytes under basal or forskolin stimulated conditions. n=6 for WT, 3 for KO and OE. l) Concentration of FFAs released into the medium of hPSC-adipocytes under basal or forskolin stimulated conditions. n=30/21 for WT, 42/42 for KO, 66/90 for OE basal/stimulated. Data are means ± SD. * = $p \leq 0.05$, ** = $p \leq 0.01$, *** = $p \leq 0.001$, **** = $p \leq 0.0001$, one- or two-way ANOVA. All n's are independent biological replicates performed in technical duplicate.

**Supplemental Figure 3. Extended data related to subcellular localization and energetic effects of MTLN, related to Figure 3.** a) Confocal microscopy depicting ATP5B (green), neutral lipids (pink), and nuclei (blue) in hPSC-adipocytes. The left panel is an exposure-matched control OE vector as a negative control indicating HA antibody background staining. The right panel is an exposure-matched secondary antibody-only image as a negative control indicating background fluorescence. Scale bar, 20 μm. b) Confocal microscopy showing MTLN-HA (red), ATP5B (green), neutral lipids (purple), and nuclei (blue) in differentiated hPSC-adipocytes in triplicate replicating experiments. Scale bar, 20 μm. c) Confocal microscopy showing MTLN-FLAG (red), HK1/ATP5B (green), neutral lipids (purple), and nuclei (blue) in hPSC-adipocytes. The right panel is an exposure-matched secondary antibody-only image as a negative control indicating background fluorescence. Scale bar, 20 μm. d) Anti-HA immunogold-labeled hPSC-adipocytes with a control OE vector serves as a negative control for transmission electron microscopy studies. e) Immunogold labeling of MTLN-HA in differentiated hPSC-adipocytes. Replicate experiments at three magnification levels are shown. f) Immunogold labeling of MTLN-FLAG in differentiated hPSC-adipocytes. Arrows point to gold particles localized at the mitochondrial membrane. g) ECAR of hPSC-adipocytes during serial stimulation with glucose, oligomycin, and 2-deoxyglucose. n=30. h) OCR of hPSC-adipocytes during serial stimulation with oligomycin, CCCP, and antimycin A/rotenone. n=30. i) OCR of hPSC-adipocytes during starvation followed by serial stimulation with palmitate, oligomycin, CCCP, and antimycin A/rotenone. n=35. j) Comparison of basal and ATP-linked respiration, as well as maximal and spare respiratory capacity of hPSC-adipocytes. n=30. k) *UCP1* and *CPT1* mRNA expression analysis of MTLN KO, WT, and MTLN OE hPSC-adipocytes. n=9. l) *ND1* and *ND5* mtDNA quantity analysis of MTLN KO, WT and MTLN OE hPSC-adipocytes. n=6 for WT and KO, 9 for OE. Data are means ± SD. * = $p \leq 0.05$, ** = $p \leq 0.01$, *** = $p \leq 0.001$, one- or two-way ANOVA. All n's are independent biological replicates performed in technical duplicate.

**Supplemental Figure 4. Extended data related to biological pathway analysis and MTLN interactions, related to Figure 4.** a) Gene ontology analysis describing the biological pathways enriched in the co-immunoprecipitated proteins bound to MTLN-Flag. Orange: mitochondrial processes. White: protein translation and overexpression. Grey: Other. Modified Fisher Exact P-Value, EASE Score. Data in Supplemental Table 4. b-d) uncropped immunoblots used in Figure 4.

Supplemental Table 4. Kegg Pathway Analysis of Immunoprecipitated Proteins, Related to Supplementary Figure 4a.

| Term | PValue | FDR |
|---|---|---|
| **Ribosome** | 2.81E-25 | 3.29E-22 |
| **Oxidative phosphorylation** | 2.94E-07 | 3.43E-04 |
| **Fatty acid metabolism** | 1.01E-06 | 0.001177483 |
| **Pyruvate metabolism** | 8.15E-06 | 0.009534287 |
| **Alzheimer's disease** | 1.26E-05 | 0.014744305 |
| **Parkinson's disease** | 1.61E-05 | 0.01885183 |
| **Valine, leucine and isoleucine degradation** | 2.03E-05 | 0.023750611 |
| **Biosynthesis of unsaturated fatty acids** | 3.56E-05 | 0.041635892 |
| **Citrate cycle (TCA cycle)** | 5.27E-05 | 0.061626906 |
| **Huntington's disease** | 5.76E-05 | 0.067281384 |
| **Propanoate metabolism** | 6.76E-05 | 0.078968375 |
| **Proteasome** | 2.19E-04 | 0.255326078 |
| **Fatty acid elongation in mitochondria** | 2.56E-04 | 0.298580235 |
| **Glycolysis / Gluconeogenesis** | 3.24E-04 | 0.378657897 |
| **Tryptophan metabolism** | 0.001928104 | 2.231394172 |
| **beta-Alanine metabolism** | 0.002633853 | 3.03670699 |
| **Butanoate metabolism** | 0.003878293 | 4.441943803 |
| **Spliceosome** | 0.011819171 | 12.97912799 |
| **PPAR signaling pathway** | 0.012556727 | 13.73555596 |
| **Pathogenic Escherichia coli infection** | 0.014189132 | 15.38839481 |
| **Limonene and pinene degradation** | 0.023492963 | 24.26852227 |
| **Glutathione metabolism** | 0.025034765 | 25.65491006 |
| **Fatty acid biosynthesis** | 0.027528922 | 27.84859109 |
| **Aminoacyl-tRNA biosynthesis** | 0.037197044 | 35.80420646 |
| **Lysine degradation** | 0.048336348 | 43.97110827 |
| **Cardiac muscle contraction** | 0.063839579 | 53.76136456 |